8/24/67

[redacted]

DECLASSIFIED-AUTHORITY,
UNITED AIRCRAFT RESEARCH LABS.
LETTER DATED 8/21/67

UNITED AIRCRAFT CORPORATION

GPO PRICE $ _____

CSFTI PRICE(S) $ _____

Hard copy (HC) 3.00

Microfiche (MF) .65

ff 653 July 65

United Aircraft Research Laboratories

EAST HARTFORD, CONNECTICUT

FACILITY FORM 602

N68-29503 (ACCESSION NUMBER) (THRU)

36 (PAGES) 1 (CODE)

CR-95730 (NASA CR OR TMX OR AD NUMBER) 22 (CATEGORY)

[redacted]

DKF

C67-3701

[redacted]

United Aircraft Research Laboratories

UNITED AIRCRAFT CORPORATION

EAST HARTFORD, CONNECTICUT

E-910093-31

Investigation of Gaseous Nuclear
Rocket Technology-Classified Programs (U)

Quarterly Progress Report No. 13-C
September 16 through December 15, 1966
Contract No. NASw-847

REPORTED BY George H. McLafferty
George H. McLafferty

[redacted] contains information affecting the national defense of the United States within the meaning of the Espionage Laws, Title 18, U.S.C., Sections 793 and 794. The transmission or the revelation of its contents in any manner to an unauthorized person is prohibited by law.

DATE December 30, 1966

NO. OF PAGES 36

COPY NO. 15

[redacted]

[redacted]

Report E-910093-31

Investigation of Gaseous Nuclear Rocket Technology -- Classified Programs (U)

Quarterly Progress Report No. 13-C - September 16 through December 15, 1966

SUMMARY

The classified portion of the investigation of gaseous nuclear rocket technology is designed to have particular application to a vortex-stabilized engine concept which is based on the transfer of heat by thermal radiation from gaseous nuclear fuel held in position by the fluid forces in a vortex to seeded hydrogen propellant passing over the fuel region. Included in these programs are theoretical and experimental studies of the fluid mechanics of vortex flow to determine criteria for fuel containment and studies of the effect of the results of these investigations on the characteristics of full-scale engines. During the thirteenth quarter, tests at high Reynolds numbers were initiated using a vortex tube employing directed wall jets for injection of the simulated propellant. Preliminary results were obtained from the rotating-peripheral-wall stability experiments and from an analysis to determine the effect of several different variables (including the substitution of hydrogen for helium as a moderator coolant) on overall engine characteristics. An analysis was also completed which relates the various measures of time constant in a vortex tube to the fuel costs in a full-scale engine.

The investigation described herein is being carried out under Contract NASw-847 with the National Aeronautics and Space Administration through the Space Nuclear Propulsion Office.

[redacted]

DISCUSSION

Vortex Fluid Mechanics Investigations

The primary objective of the FY 1967 vortex fluid mechanics investigations is to determine whether the fuel containment characteristics that were measured in preceding tests can be improved. A new directed-wall-jet vortex tube for use in the high Reynolds number test facility was put into operation during this report period. This will allow testing of directed-wall-jet configurations having tube length-to-diameter ratios from 1.0 to 3.0 at axial-flow Reynolds numbers corresponding to a full-scale engine. While the new vortex tube was being constructed, additional two-component gas tests were conducted with the test equipment used in the FY 1966 research program. Experiments directed toward increased understanding of the stability of vortexes with and without superimposed axial flow were continued using the rotating stability water-vortex apparatus.

New Directed-Wall-Jet Vortex Tube

A new directed-wall-jet vortex tube was designed, constructed and installed in the high-Reynolds-number (HRN) test facility. Previous tests of directed-wall-jet (DWJ) configurations were conducted at axial-flow Reynolds numbers below approximately 100,000 and at only one vortex tube length-to-diameter ratio (L/D = 3.0). The new vortex tube will allow testing at axial-flow Reynolds numbers up to approximately 500,000 using air as the light gas. The position of the nonaxial-flow end wall can be adjusted to provide values of L/D from 1.0 to 3.0.

The light-gas injection system is similar to that used in the previous tests with directed-wall jets (see Fig. 1 of Quarterly Progress Report No. 10-C). The vortex tube is 10 in. in diameter and 30 in. long and has 900 individually directable injection ports spaced uniformly on the peripheral wall. The flow enters an injection port through one of 15 separate plenums surrounding the vortex tube. Each plenum supply pipe has its own flow meter and control valve. The light gas is injected essentially tangent to the peripheral wall of the vortex tube and can have both circumferential and axial components of injection velocity. Total injection port areas up to 45 $in.^2$ are attainable using ports having different injection slot heights. Measurements of heavy-gas time constant are made using the "radial traverse" method employed in the FY 1966 high-Reynolds-number gas-vortex tests (see description in Quarterly Progress Report No. 12-C).

Shakedown tests with the new directed-wall-jet vortex tube were completed and initial routine tests were initiated. These initial tests employ an L/D = 3.0 configuration having the most promising light-gas injection distribution tested to date (injection angle variation from β_j = 0 deg, or no axial component, at the

nonaxial-flow end wall to β_j = 63.5 deg at the axial-flow end wall; see Table I and Fig. 3 of Quarterly Progress Report 12-C). The tests will cover the range from low axial-flow Reynolds numbers up to approximately 500,000 using air as the light gas. Subsequent tests will include (1) tests with configurations having L/D = 1.0 and 2.0, (2) tests employing helium as the light gas, (3) tests with an intermediate gas buffer layer between the heavy and light gases, and (4) tests with flow withdrawal through the center of the axial-flow end wall to create a radial-inflow type of vortex.

Measurements of Heavy-Gas Time Constants

Tests Employing Multiple-Fixed-Port Vortex Tubes

Additional tests were conducted in the high-Reynolds-number test facility using the multiple-fixed-port vortex tubes fabricated for the FY 1966 research program. These three vortex tubes were described in Quarterly Progress Report No. 12-C; a typical tube is shown in Fig. 1A. Light gas is injected without an axial component of velocity through 4284 holes drilled at an angle of approximately 19 deg with respect to the local tangent to the peripheral wall. The total injection port areas of the vortex tubes are A_j = 13.1, 20.5, and 40.2 in.^{2}. In all tests, air was used as the light gas, and a fluorocarbon (FC-77) was used as the heavy gas.

The objectives of these tests were:

(1) To determine the effect of changes in axial-flow Reynolds number on heavy-gas containment in multiple-fixed-port vortex tubes for values of $Re_{z,w}$ up to approximately 500,000, and

(2) To obtain preliminary data on the effect of changes in vortex-tube length-to-diameter ratio on heavy-gas containment.

Data for the three L/D = 3.0 configurations are presented in Figs. 2 through 4. Data for the L/D = 1.0 configuration (i.e., the L/D = 3.0 vortex tube having an injection area of A_j = 40.2 in.^{2} with the axial-flow end wall relocated at 10 in. from the nonaxial-flow end wall) is presented in Fig. 5. The dimensionless time constant decreased with increasing heavy-gas density ratio and with increasing axial-flow Reynolds number. These trends have been observed in all previous tests.

The effects of changes in axial-flow Reynolds number on the dimensionless time constants for these four configurations are shown in Fig. 6. This figure was obtained by crossplotting the data appearing in Figs. 2 through 5 at a heavy-gas density ratio of $\bar{\rho}_{F_1}/\rho_{P_1}$ = 0.2. Also shown in Fig. 6 are lines indicating the variation of the minimum dimensionless time constant (for the light-gas and heavy-gas fully mixed before entering the vortex tube) with $Re_{z,w}$ for the two values of L/D.

[redacted]

The minimum dimensionless time constant varies directly with L/D and inversely with $Re_{z,w}$; i.e., $\tau_{F_1} / \tau_{F_{1_{MIN}}} \sim (L/D)/Re_{z,w}$.

Several conclusions may be drawn from Fig. 6. First, for all three L/D = 3.0 configurations, it appears that the dimensionless time constant, τ_{F_1}, decreases at approximately the same rate as the minimum value, $\tau_{F_{1_{MIN}}}$, with increasing $Re_{z,w}$. This is more evident in Fig. 7 where the ratio $\tau_{F_1} / \tau_{F_{1_{MIN}}}$ is between 2 and 4 for all three vortex tubes over the complete range of axial-flow Reynolds numbers. It will also be noted that the injection area, and hence the ratio of the average axial velocity in the vortex to the average light-gas injection velocity $\bar{V}_{z,w}/V_j$, appears to have no significant effect on containment.

For the L/D = 1.0 configuration, the dimensionless time constants were less than those for the L/D = 3.0 configurations at values of $Re_{z,w}$ less than about 200,000 (Fig. 6) and were about equal at values of $Re_{z,w}$ above 200,000. As indicated in Fig. 7, $\tau_{F_1} / \tau_{F_{1_{MIN}}}$ increased from about 5 at $Re_{z,w}$ = 50,000 to about 9 at $Re_{z,w}$ = 400,000 for the L/D = 1.0 configuration. This difference in the trend with increasing $Re_{z,w}$ may be significant and it will be investigated further using the new directed-wall-jet vortex tube in the next series of tests.

Figure 8 is a revised version of the correlation of $\tau_{F_1} / \tau_{F_{1_{MIN}}}$ with $\bar{V}_{z,w}/V_j$ that was presented in Fig. 6 of Quarterly Progress Report No. 12-C. All data presented in Fig. 8 were obtained using configurations in which the heavy gas was injected at the center of the nonaxial-flow end wall, whereas Fig. 6 of Quarterly Progress Report No. 12-C contained data obtained using configurations having three different heavy-gas injection configurations. The apparent trend of decreasing $\tau_{F_1} / \tau_{F_{1_{MIN}}}$ with increased $\bar{V}_{z,w}/V_j$ discussed in Quarterly Progress Report No. 12-C has not been substantiated in recent tests with heavy-gas injection only through the center of the nonaxial-flow end wall. The data presented in Fig. 8 show that, for heavy-gas injection at the center of the nonaxial-flow end wall, there was no significant effect of $\bar{V}_{z,w}/V_j$ on $\tau_{F_1}/\tau_{F_{1_{MIN}}}$. It is also important to note that at this axial-flow Reynolds number ($Re_{z,w}$ = 50,000) and heavy-gas density ratio ($\bar{\rho}_{F_1} / \rho_{P_1}$ = 0.15), the two configurations having the highest containment parameters were (1) directed-wall-jet injection with L/D = 3.0 and injection angle variation from 0 to 63.5 deg (see Fig. 1B), and (2) multiple-fixed-port injection with L/D = 1.0. This has been taken into consideration in planning the initial tests to be conducted using the new directed-wall-jet vortex tube.

Results of tests to determine the effect of axial-flow exhaust annulus geometry on the containment characteristics of the L/D = 3.0 configuration having A_j = 13.1 $in.^2$ are shown in Fig. 9. In these tests, the inner radius of the exhaust annulus was changed and the struts in the axial-flow exhaust plenum (normally present) were removed. The results indicate that there were no appreciable effects of these changes on the containment characteristics of the flow.

[redacted]

Tests Employing Heavy-Gas Injection with Swirl

The directed-wall-jet test facility constructed for the FY 1966 research program was also used for additional tests during this report period. This facility was described in Quarterly Progress Report No. 12-C; the L/D = 3.0 directed-wall-jet vortex tube used in these tests is shown in Fig. 1B. Light gas is injected with both tangential and axial components of velocity through 600 directable wall jets. For these tests the angle of injection varied from 0 deg (no axial component) at the nonaxial-flow end wall to 45 deg at the axial-flow end wall. The tangential component of injection velocity and mass flow per unit length were approximately uniform along the length of the tube for all tests. The total light-gas injection area was $A_j = 9.7$ in.^{2}.

Heavy-gas time constants were measured for a configuration in which the heavy gas was injected with swirl near the center of the nonaxial-flow end wall. Details of the heavy-gas injection configuration tested are presented in the table in Fig. 10. Both the new data and previous data for heavy-gas injection without swirl from a duct at the center of the nonaxial-flow end wall are shown in Fig. 10 for comparison. The data for heavy-gas swirl injection show a moderate increase in $\tau_{F_1}/\tau_{F_{1MIN}}$ compared with the data without swirl for heavy-gas density ratios above about 0.2. However, this increase is not sufficiently large to indicate that the flow has been significantly altered.

Summary of Principal Results

A series of flow visualization tests was conducted with radial outflow and superimposed axial flow. Flow patterns were examined for various combinations of axial-flow Reynolds number ($Re_{z,w}$), radial Reynolds number (Re_r), outer tube rotation rate, inner tube rotation rate, and stationary and rotating end walls. The principal result of the tests was that the combination of large $\bar{V}_{z,w}/V_\phi$ and large $Re_{z,w}$ produced unstable flow, while the combination of small $\bar{V}_{z,w}/V_\phi$ and small $Re_{z,w}$ produced stable flow. Stable flow was observed only for values of $Re_{z,w}$ less than 3000 and values of $\bar{V}_{z,w}/V_\phi$ less than 0.02. It is also significant to note that these preliminary results indicate unstable flow would be expected at the combinations of $\bar{V}_{z,w}/V_\phi$ and $Re_{z,w}$ used in the two-component-gas vortex tests.

Axial-flow tests at a value of $Re_{z,w}$ of 16,000 and values of $\bar{V}_{z,w}/V_\phi$ of 0.20 and 0.25 were also conducted with radial inflow by removing the centerline porous tube and by withdrawing flow through the port in the centerline of the axial-flow end wall at a radial Reynolds number of 90. The flow was stable with stationary or rotating end walls, whereas tests with radial outflow at the same values of $Re_{z,w}$ and $\bar{V}_{z,w}/V_\phi$ were unstable. The stability of the radial inflow configuration could be destroyed, however, by injecting flow through a port in the center of the nonaxial-flow end wall. The injection radial Reynolds number required to cause turbulence was -45 and -60 for rotating and stationary end walls, respectively.

[redacted]

Testing of the basic vortex configuration (no superimposed axial flow) with radial outflow was resumed to obtain tangential velocity profiles by the particle-trace method. However, at the present time, only one tangential velocity profile has been obtained due to mechanical difficulties that developed in the rotating stability apparatus. A modification was required to eliminate an eccentricity of the driving shaft. The apparatus was inoperative for a period of four weeks while the modification was completed.

The single tangential velocity profile obtained (for $Re_r = -30$ with the end walls and outer tube rotating together) is shown in Fig. 11. Also shown is a profile obtained in the 2144-port-injection vortex tube (all walls fixed; see Ref. 1). In the 2144-port tube, the vortex was driven by jets at the peripheral wall; flow was injected through the centerline porous tube, and flow was withdrawn through bypass ducts at the peripheral wall. In the rotating stability apparatus, flow was injected through the centerline porous tube and was withdrawn through the rotating wall. The net outflow radial Reynolds number in both cases was $Re_r = -30$. There is essentially no difference in the tangential velocity profiles; however, there was a radical difference in the appearance of the two flows. The flow in the 2144-port-injection vortex tube was turbulent everywhere, while the flow in the rotating stability apparatus was laminar everywhere, including in the end-wall boundary layers (see Fig. 11 of Quarterly Progress Report 12-C). The observed flow pattern with the same Re_r, but with stationary end walls (see Fig. 11 of Quarterly Progress Report No. 12-C), was laminar to a radius of about 2.5 in. and turbulent at larger radii. This indicates that the method of driving the vortex (i.e., whether jets at a fixed wall or a rotating outer wall) has considerable influence on the stability of the flow.

A sketch of the streamlines for a typical laminar, radial-outflow case as obtained from flow visualization observations of dye patterns in the r-z plane is shown in Fig. 12. This sketch is for fluid injection through a stationary inner porous tube and for end walls rotating with the outer tube. A description of this flow was given in Quarterly Progress Report No. 12-C. The location of the inner stagnation radius is a unique function of Re_r and Re_ϕ (i.e., the outer tube rotational speed). At constant Re_r the inner stagnation radius decreases with increasing Re_ϕ; at constant Re_ϕ the inner stagnation radius increases with increasingly negative values of Re_r (i.e., with more fluid injected through the porous tube). This occurs only for laminar flows. For this flow configuration, completely laminar flows were observed to occur for $Re_r > -37$. However, at $Re_r = -37$, periodic transition to turbulent flow was observed (that is, alternately laminar and turbulent flow) in the right end-wall boundary layer at a radius of about 3 in. This turbulence, in turn, caused portions of the primary flow to become turbulent. The axial extent and the duration of the observed turbulence varied with outer-tube rotational speed. For example, at a rotational speed of 40 rpm ($Re_\phi = 67{,}000$), the axial extent of the turbulence from the right end wall was about 5 in., and the duration of the turbulence was about 50 sec; the duration of the laminar flow was about 90 sec. The remaining portions of the vortex flow, including the left-end

wall boundary layer, remained laminar. As rotational speed was increased, the axial extent and duration of turbulence was increased. At $Re_r < -37$, turbulence occurred continuously near the right end wall. Its axial extent was a function of rotational speed; the other portions of the flow remained laminar.

Future efforts in the basic vortex configuration will be directed toward completion of the particle-trace tests to obtain tangential velocity profiles.

Engine Design

Three modifications to the specific gaseous nuclear rocket engine configuration as presented in Ref. 2 were investigated to determine their effects on overall design and performance. These modifications were (1) replacement of the tungsten liner tubes with pyrolytic-graphite-coated beryllium tubes, (2) elimination of the heavy water moderator, and (3) substitution of hydrogen for helium in the moderator coolant circuit. The specific combinations of these modifications which were investigated are listed in Table I. Configuration A represents the original design of Ref. 2, Configuration B incorporates modification (1) above; Configuration C incorporates modifications (1) and (2), Configuration D incorporates modifications (1) and (3); and Configuration E incorporates all three of the modifications. The effects on the moderator configuration, operating conditions, and engine weight, exclusive of pressure vessel, are discussed.

Beryllium Liner Tubes

The use of beryllium liner tubes reduces the amount of tungsten in the inner liner region and eliminates the bimetallic tungsten-beryllium joints where the tubes join the beryllium liner. The basic configuration of the liner tubes is similar to the original design and is shown in Fig. 8 of Ref. 2.

Because of the high cavity wall temperatures (~ 5000 R) and the high radiant and convective heat flux (~ 2360 Btu/sec-ft^2), the beryllium tubes must be surrounded by an insulator such as pyrolytic graphite. The pyrolytic graphite is coated with niobium carbide to protect it from the hot hydrogen in the cavity. It is assumed that the pyrolytic graphite is deposited on the beryllium tubes in such a manner that the thermal conductivity is low in the radial direction ($\sim 1.8 \times 10^{-4}$ Btu/sec-ft-deg R) and is high in the circumferential direction ($\sim 1.7 \times 10^{-2}$ Btu/sec-ft-deg R). The ratio of pyrolytic graphite thickness to half circumference is on the order of 0.3, and a comparison of the quotient of the thermal conductivity and distance predicts a relatively uniform circumferential temperature distribution. The entire surface area of the liner tube was used as a heat transfer area in the calculation of the film temperature drop and the required tube diameter.

A comparison of the design characteristics of the liner tubes for the various configurations is shown in Table II. The operating conditions for the beryllium tube configurations are based on a maximum beryllium temperature of 1500 R.

Referring to Configuration B, where helium is used as a moderator coolant and the heavy water moderator is present, the calculations predict an extremely high pressure loss in the tubes. The pressure of the heavy water moderator establishes a minimum inlet temperature to the tubes of 900 R and allows only 600 R for a film temperature drop in the tubes. The required film temperature drop can be achieved only by a small tube diameter ($\sim$ 0.031 in.) with a high dynamic pressure ($\sim$ 8 atm) or a change in tube length which would modify the inner liner configuration. If the heavy water is removed, the inlet temperature is reduced to 564 R and the resulting configuration is shown as Configuration C.

If hydrogen is used as a coolant, the total pressure loss in the tubes decreases by a factor of 10, and the beryllium tubes could be used with the heavy water present (Configuration D) or with the heavy water removed (Configuration E).

Elimination of Heavy Water Moderator

The heat generated in the heavy water region of the moderator is approximately 9.0×10^5 Btu/sec and, since the heavy water must be maintained at a temperature below 1000 R, it represents a relatively low-temperature heat source. The heavy water must be cooled by the moderator coolant before it enters the liner tubes, and the combined heat from the pressure vessel and the D_2O raises the coolant inlet temperature to 903 R. Elimination of the D_2O lowers the tube inlet temperature to 564 R, eliminates the D_2O heat exchangers and circulation system, and eliminates the outer containment shell of the D_2O region. The thickness of the beryllium oxide and graphite regions is increased in order to maintain the 4500 R outlet temperature.

The characteristics of the moderator region with the heavy water removed (Configurations C and E) are compared with the design of Ref. 2 in Table III. In addition to the weight saving in the solid moderator which is shown in the table, there is a decrease of 4.3 in. in the inside radius of the pressure vessel which would reduce the pressure vessel weight.

Substitution of Hydrogen as a Moderator Coolant

The use of hydrogen as a moderator coolant permits a reduction of a factor of 3.2 in the moderator coolant flow rates if the temperature levels are maintained at the same levels as specified in the preliminary design. This reduction in flow rate is more than enough to offset the decreases in fluid density, and the dynamic pressure is reduced by a factor of 5 to 10 depending on the fluid temperature. If all of the cooling hole and piping dimensions are held constant, the total coolant pressure drop would be reduced from 35 to 7 atm and the pumping power requirements

reduced. Another alternative is to reduce the piping and heat exchanger dimensions in order to reduce the engine weight. A comparison of piping sizes and weights is shown in Table IV. A redesign of the high-temperature heat exchanger showed a 40 percent reduction in the weight was possible with a hydrogen moderator coolant.

The use of hydrogen as a moderator coolant makes it necessary to coat the graphite moderator with niobium carbide in order to protect it from attack by the hot hydrogen. The quantity of niobium carbide necessary as a function of pressure drop in the graphite region is shown in Fig. 13. This plot is based on the graphite thickness used in engine Configuration D (8.7 in.) and a 0.002 in. niobium carbide coating on the cooling hole surfaces. In addition to the niobium carbide on the cooling passages, approximately 15 lb are required to coat the graphite in the region of the propellant and coolant inlets.

Total Engine Weight

A comparison of total engine weight exclusive of pressure shell for the configurations investigated is shown in Table V. In addition to total weights, the absorbing area of the tungsten-184 and niobium carbide are listed to show the relative amounts of neutron absorbing materials present in the various configurations.

Configurations C and E have a smaller outside diameter than the preliminary design and would have additional weight reductions in the pressure vessel.

Criticality Calculations

Criticality calculations were made for a modification of the engine design of Ref. 3 in which the size of the exhaust nozzle approach slot was reduced by a factor of 2. Two-dimensional diffusion theory calculations indicated a critical mass for this configuration of 43.1 lb. This mass compares well with a predicted critical mass of 42.2 lb from Ref. 3 based on interpolation from the other configurations.

Work on estimating the critical mass requirements for the four engine modifications described in the preceding section was initiated. The replacement of the tungsten-184 liner tubes with niobium carbide coated, pyrographite insulated, beryllium tubes and redesign of moderator dimensions has required the calculation of additional neutron cross section libraries. Twenty-four-group cross sections have been calculated for niobium carbide and one-dimensional diffusion theory calculations are underway from which 4-group cross sections will be produced for the new reflector-moderator configurations for later use in 2-D criticality calculations.

Interpretation of Fuel Loss Rate Parameters

Criteria for Acceptable Fuel Loss Rate

In the following discussion, it is assumed that economics will govern the minimum acceptable loss rate of nuclear fuel from a gaseous nuclear rocket engine. In determining this acceptable fuel loss rate, it is necessary to specify a mission for the engine. In the following discussion, the mission considered will be that of Ref. 4 in which the gaseous-nuclear-rocket-powered vehicle is boosted by a Saturn I-C launch vehicle, after which the gaseous nuclear rocket engine is employed to accelerate the vehicle into orbit and thence to a velocity 50,000 ft/sec greater than orbital velocity. It is assumed that there is one gaseous nuclear rocket engine stage and two tankage stages. The engine considered in the analyses is assumed to have the following characteristic (see Refs. 1, 2, and 3): Specific impulse, 2150 sec; thrust, 1.24×10^6 lb; weight, 1.24×10^5 lb; fuel density ratio, 5.0; and cavity pressure, 1000 atm. The conditions in the cavity of this engine are given in Table VI. According to Fig. 76 of Ref. 4, this engine could be used to accelerate a payload of 285,000 lb through the velocity increment considered. If there were no loss of nuclear fuel, the total propellant consumed by the gaseous nuclear rocket would be approximately 875,000 lb, and the cost would be $225 per lb of payload on the basis of the information in Fig. 100 of Ref. 4.

The permissible fuel loss rate must be judged on the basis of the difference in mission costs calculated using gaseous nuclear rockets and solid-core nuclear rockets. According to Table V of Ref. 4, the cost of using four stages of solid-core nuclear rockets in a suborbit-start mode would be $2,426 per lb of payload for the same mission considered for the gaseous nuclear rocket. Thus the potential savings that could be accrued by using a gaseous-core nuclear rocket providing perfect containment rather than solid-core nuclear rockets is $2,426 minus $225 or $2,201 per lb of payload. Since the payload for the gaseous nuclear rocket is 285,000 lb, the absolute savings per flight would be $\$6.28 \times 10^8$.

The first reference point for fuel loss rate in a gaseous nuclear rocket is calculated on the basis that the total cost per pound of payload would be the same for the gaseous nuclear rocket as for the solid-core nuclear rocket. If the fuel cost is assumed to be $7,000 per lb (as in Ref. 4), this break-even criteria would permit loss of 89,700 lb of nuclear fuel. Therefore, the ratio of the total propellant employed to total fuel loss would be 875,000/89,700 or 9.76. The actual ratio of propellant flow to fuel flow would have to be considerably greater than this value in order to justify the development of a gaseous nuclear rocket.

Next, assume that the costs associated with the flight of a gaseous nuclear rocket must be one-third of those for a solid-core nuclear rocket in order to justify engine development. Thus the cost per pound of payload would be 2426/3 or $808 per lb of payload. The allowable cost of the fuel would be $808 minus $225 or

[redacted]

$583 per lb of payload, or $1.66 x 10^8. Proceeding as before, the total fuel loss would be $(1.66 \times 10^8)/(7000)$ or 23,700 lb, and the ratio of the total propellant used to fuel loss would be 875,000/23,700 or 36.9.

Interpretation of Acceptable Fuel Loss Rates in Terms of Time Constant Parameters

A number of different fuel loss rate parameters have been employed in the fluid mechanics tests described in Refs. 5 and 6 (see also preceding section). One of these is the fuel time constant parameter, t_F, which is defined as the fuel stored (18.1 lb for the conditions of Table VI) divided by the fuel flow rate. Fuel or heavy-gas time constants measured in the fluid mechanics tests of Refs. 5 and 6 have been made dimensionless by dividing by the parameter $(\rho/\mu)r_1^2$. In interpreting these dimensionless fuel time constants in terms of the characteristics of a full-scale engine, it is necessary to select the value of ρ/μ which has the greatest influence on the fuel loss rate in the full-scale engine. The studies of Ref. 4 employed a value of ρ/μ determined on the basis of the propellant characteristics at the centerline temperature and the fuel cavity pressure. As noted in Table VI, the resulting definition of $(\rho/\mu)r_1^2$ provides a value of fuel time constant parameter of 1195 sec. It is also possible to define the fuel time constant parameter on the basis of ρ/μ at the outside edge of the fuel-containment region (Station 6). This second choice of ρ/μ provides a value of $(\rho/\mu)r_1^2$ of 2820 sec as noted in Table VI.

Some of the data in Refs. 5 and 6 has also been plotted in terms of the ratio of fuel time constant to a minimum time constant determined on the basis of complete mixing of the fuel and propellant at injection. In converting values of $t_F/t_{F_{MIN}}$ from model tests to full-scale engines, it is also necessary to make a choice as to the density employed in calculating volume flow. In Table VI, this volume flow, Y_6, was determined by dividing the cavity propellant flow by the density at Station 6. As noted by the last item in Table VI, the resulting minimum time constant determined by dividing the cavity volume by the volume flow is equal to 0.01546 sec.

The interrelation between various parameters which are a measure of fuel loss rate or containment time and various criteria for containment is given in Table VII. In addition to the economics criteria determined in the preceding subsection, all parameters are calculated on the basis of three additional criteria: fully-mixed flow, a value of $\tau_{F_{1-8}}$ of 0.01, and a ratio of propellant flow to fuel flow of 10^3. The parameters $t_{F_{MIN}}$, $(\rho/\mu)_6 r_1^2$, $(\rho/\mu)_8 r_1^2$, W_F and W_T used in evaluating Columns ② through ⑥ of Table VII were obtained from Table VI. The constant employed in evaluating Column ⑦ was obtained by multiplying the cost per pound of fuel ($7,000 per lb) by the propellant consumed (875,000 lb) and dividing by the payload (285,000 lb). The reduction in hydrogen propellant weight resulting from the weight of the fuel required (i.e., the change in specific impulse due to the change in molecular weight) is neglected. The constant of 225 used in evaluating Column ⑧

represents the costs exclusive of the fuel costs. The economic criteria which states that the costs must be one-third of those associated with a solid-core nuclear rocket lead to values of $t_F/t_{F_{MIN}}$ of 75.0 or a value of $\tau_{F_{1-e}}$ of 0.000971 at an axial-flow Reynolds number of 480,000.

An analysis similar to that described in the preceding paragraphs for the suborbit-start mission profile was also carried out for an orbit-start mission profile. If there was no loss of fuel from the gaseous nuclear rocket, the cost per pound of payload with orbit start would be $578 per lb of payload on the basis of using the same engine, the same payload, and the same required velocity increment beyond orbit as for the suborbit-start profile. According to Table V of Ref. 4, the costs with orbit start using solid-core nuclear rockets would be $2,703 per lb of payload. The required ratio of fuel time constant to minimum fuel time constant to provide overall mission costs equal to those for a solid-core nuclear rocket and equal to one-third of those for a solid-core nuclear rocket would be 11.0 and 97, respectively (the corresponding numbers for suborbit start are 19.2 and 75.0, respectively, according to Table VII).

Comparison of Measured and Required Fuel Time Constants

The values of the ratio of heavy-gas time constant to minimum heavy-gas time constant which have been measured to date (see Figs. 1 through 10) are less than those required to provide overall mission costs equal to those for a solid-core nuclear rocket, and substantially less than those required to provide mission costs equal to one-third of the mission costs for a solid-core nuclear rocket (see Table VII). It is expected that the new configurations which will be employed in the new directed-wall-jet vortex tube will provide substantial increases in heavy-gas time constant relative to those which have been obtained to date, although it is not known whether these increases will be sufficient to lead to an economic justification for developing a gaseous nuclear rocket of the type described in Refs. 1 through 3. However, the investigations of the fluid mechanics of vortex flow also provide results which are applicable to the nuclear light bulb engine described in Ref. 7. As noted in Ref. 7, the required values of axial-flow Reynolds number and heavy-gas density ratio for a nuclear light bulb engine are on the order of 15,000 and 0.1, respectively. These values are well within the values which can be obtained with laminar flow in a radial inflow type of vortex.

REFERENCES

1. Travers, A.: Experimental Investigation of Peripheral-Wall Injection Techniques in a Water Vortex Tube. UARL Report D-910091-7, prepared under Contract NASw-847, September 1965. Unclassified.

2. McLafferty, G. H., H. E. Bauer, and D. E. Sheldon: Preliminary Conceptual Design Study of a Specific Vortex-Stabilized Gaseous Nuclear Rocket Engine (U). UARL Report E-910093-29, prepared under Contract NASw-847, September 1966. Confidential.

3. Latham, T. S.: Nuclear Criticality Study of a Specific Vortex-Stabilized Gaseous Nuclear Rocket Engine (U). UARL Report E-910375-1, prepared under Contract NASw-847, September 1966. Confidential.

4. McLafferty, G. H.: Analytical Study of the Performance Characteristics of Vortex-Stabilized Gaseous Nuclear Rocket Engines (U). UARL Report D-910093-20, prepared under Contract NASw-847, September 1965. Confidential.

5. Mensing, A. E., and J. S. Kendall: Experimental Investigation of Containment of a Heavy Gas in a Jet-Driven Light-Gas Vortex (U). UARL Report D-910091-4, prepared under Contract NASw-847, March 1965. Confidential.

6. Mensing, A. E., and J. S. Kendall: Experimental Investigation of the Effect of Heavy-to-Light-Gas Density Ratio on Two-Component Vortex Tube Containment Characteristics (U). UARL Report D-910091-9, prepared under Contract NASw-847, September 1965. Confidential.

7. McLafferty, George H.: Characteristics of a Gaseous Nuclear Rocket Engine Employing Transparent-Wall Containment (U). Report UAR-D40, March 1965. Also presented as a paper at the AIAA Nuclear Propulsion Specialists Conference at the Air Force Academy, June 14-18, 1965. Confidential.

[redacted]

[redacted]

LIST OF SYMBOLS

$A_{F,j}$	Heavy-gas injection area, ft^2 or $in.^2$
A_j	Light-gas injection area at vortex tube periphery, ft^2 or $in.^2$
D	Diameter of gas vortex tube or engine cavity, $2r_1$, ft or in.
L	Length of vortex tube or engine cavity, ft or in.
N_1	Outer tube angular speed, rpm
P	Cavity pressure, atm
ΔP	Pressure drop in external piping or moderator coolant holes, atm
q	Dynamic pressure in external piping or moderator coolant holes, atm
Q_p	Volumetric flow rate of light gas, ft^3/sec
Q_T	Volumetric flow rate through thru-flow ports, ft^3/sec
Q_Z	Volumetric flow rate through axial-flow exhaust annulus, ft^3/sec
r	Radial distance from centerline of vortex tube, ft or in.
r_1	Radius of vortex tube, ft or in.
Re_d	Reynolds number based on diameter of external piping or moderator coolant hole
Re_r	Radial Reynolds number (negative for radial outflow), $Q_T/2\pi\nu L$, dimensionless
Re_z	Axial-flow Reynolds number in full-scale engine (see Ref. 4)
$Re_{z,w}$	Equivalent axial-flow Reynolds number, $Q_z/(7/16)\pi r_1 \mu_{P_1}$
$Re_{\phi,j}$	Light-gas or water tangential injection Reynolds number, $\rho_{P_1} V_{\phi,j} r_1/\mu_{P_1}$, dimensionless
t_f	Heavy-gas or fuel time constant, w_F/W_F
$t_{F_{6_{MIN}}}$	Minimum time constant based on ρ_6, sec

[redacted]

LIST OF SYMBOLS (cont'd)

T_6	Temperature at outside edge of fuel-containment region, deg R
T_8	Centerline temperature, deg R
V	Volume of vortex tube, ft^3
V_j	Average light-gas injection velocity, Q_p/A_j, ft/sec
$\bar{V}_{z,w}$	Average velocity through axial-flow annulus, $Q_z/(7/16)\pi r_1^2$, ft/sec
V_ϕ	Tangential velocity, ft/sec
$V_{\phi,j}$	Tangential component of light-gas injection velocity, ft/sec
W_C	Cavity propellant flow, lb/sec
W_F	Heavy gas or fuel flow rate, lb/sec
W_T	Total propellant flow, lb/sec
w_F	Amount of heavy gas stored in vortex tube or amount of fuel stored in engine cavity, lb
X	Cavity volume, ft^3
Y_6	Cavity volume flow based on ρ_6, ft^3/sec
β_j	Angle between r-ϕ plane and centerline of light-gas injection jet, deg
μ_{P_1}	Viscosity of light gas at vortex tube periphery, lb/sec-ft
μ_6	Viscosity at outside edge of fuel-containment region, lb/sec-ft
μ_8	Viscosity of propellant at centerline conditions, lb/sec-ft
ν	Kinematic viscosity, ft^2/sec
$\bar{\rho}_{F_1}$	Volume-averaged heavy-gas density, w_F/V, lb/ft^3
ρ_{P_1}	Light-gas density at vortex tube periphery, lb/ft^3
ρ_6	Density at outside edge of fuel-containment region, lb/ft^3

LIST OF SYMBOLS (cont'd)

ρ_8	Density of propellant at centerline conditions, lb/ft^3
τ_{F_i}	Dimensionless heavy-gas time constant, $t_f \mu_{P_i} / \rho_{P_i} r_i^2$, dimensionless
$\tau_{F_{i_{MIN}}}$	Value of τ_{F_i} calculated for complete mixing of light and heavy gases
ϕ	Azimuth angle

TABLE I

DESIGNATION OF VARIOUS ENGINE CONFIGURATIONS INVESTIGATED

Engine Configuration	Structural Material in Liner Tubes	Moderator Coolant	Heavy Water Moderator	Remarks
A	Tungsten-184	Helium	Yes	Original design configuration Ref. 2
B	Beryllium	Helium	Yes	
C	Beryllium	Helium	No	D_2O replaced by additional graphite
D	Beryllium	Hydrogen	Yes	
E	Beryllium	Hydrogen	No	D_2O replaced by additional graphite

TABLE II

COMPARISON OF LINER TUBE CONFIGURATIONS

Engine Configuration (Refer to Table I)	A	B	C	D	E
Tube Material	W-184	Be	Be	Be	Be
Coolant	He	He	He	H_2	H_2
Tube Inside Diameter, in.	0.165	0.031	0.055	0.031	0.055
Tube Wall Thickness, in.	0.010	0.005	0.005	0.005	0.005
Pyrolitic Graphite Thickness, in.	-	0.048	0.048	0.048	0.048
Niobium Carbide Thickness, in.	-	0.002	0.002	0.002	0.002
Tube Outside Diameter, in.	0.185	0.141	0.165	0.141	0.165
Number of Tubes	6.09×10^4	8.1×10^4	6.28×10^4	8.1×10^4	6.28×10^4
Coolant Flow per Tube, lb/sec	1.945×10^{-2}	1.635×10^{-2}	1.821×10^{-2}	1.635×10^{-2}	1.821×10^{-2}
Coolant Specific Heat, Btu/lb-°R	1.25	1.25	1.25	3.37	3.37
Inlet Temperature, °R	903	903	564	903	564
Outlet Temperature, °R	1175	1175	845	1175	845
Total Pressure Loss, atm	0.1	35	3.5	3.4	0.34
Total Tube Weight, lbs	566	1246	1246	1246	1246
Tungsten-184	566	-	-	-	
Beryllium	-	79	79	79	79
Pyrolytic Graphite	-	945	945	945	945
Niobium Carbide	-	222	222	222	222

[redacted]

TABLE III

COMPARISON OF MODERATOR CONFIGURATIONS WITH AND WITHOUT HEAVY WATER REGION

Engine configuration A,B,D - with heavy water region
Engine configuration C,E - no heavy water region

Engine Configuration	Radial Thickness of Region - in.		Radius at Outside of Region - in.		Volume of Region, Ft^3		Material Volume, Ft^3		Void Fraction		Summation of Volume, Ft^3		Density, lb/ft^3	Weight, lb	
	A,B,D	C,E	A,B,D	C,E	A,B,D	C,E	A,B,D	C,E	A,B,D	C,E	A,B,D	C,E		A,B,D	C,E
Cavity	36.0	36.0	36.0	36.0	170	170	0	0	1.0	1.0	170	170			
Liner Tubes	0.63	0.63	36.63	36.63	9.0	9.0	0.47	0.47	0.95	0.95	179	179	-	Refer to Table I	
Beryllium Liner	0.30	0.30	36.93	36.93	4.5	4.5	3.9	3.9	0.16	0.16	183.5	183.5		No Change	
Plenum	0.30	0.30	37.23	37.23	4.5	4.5	0	0	1.0	1.0	188.0	188.0			
Beryllium Oxide	3.50	4.00	40.73	41.23	59	66.85	50.5	58.1	0.144	0.144	247	254.4	188.5	9,530	10,980
Plenum	0.10	0.10	40.83	41.33	1.8	2.14	0	0	1.0	1.0	248.8	256.5			
Graphite	8.70	14.15	49.53	55.48	194	373.8	170.2	327.0	0.123	0.123	442.8	620.3	100.1	17,100	32,800
Plenum	0.30	0.30	49.83	55.78	8.0	10.18	0	0	1.0	1.0	450.8	630.5			
Beryllium Wall	0.30	0.30	50.13	56.08	8.2	10.54	8.2	10.54	0	0	459.6	641.0	115.4	950	1,220
Heavy Water	9.95	0	60.08	-	330.3	0	297.3	0	0.103	-	789.6	-	63.0	18,750	0
Beryllium Wall	0.30	0	60.38	-	10.46	0	10.46	0	0	0	800	-	115.4	1,210	0
Heat Exch & Piping	10.0	10.0	70.38	66.08	585	407.36	31.7	22.4	0.945	0.945	1385	1048.4			

Total weight reduction in solid moderators for configurations C & E = 2,540 lbs

[redacted]

TABLE IV

COMPARISON OF EXTERNAL PIPING CONFIGURATIONS
WITH HELIUM AND HYDROGEN MODERATOR COOLANT

Engine configuration A,B,C - helium coolant
Engine configuration D,E - hydrogen coolant

Engine Configuration	Inlets		Outlets		Connecting Pipes	
	A,B,C	D,E	A,B,C	D,E	A,B,C	D,E
ID, in.	2	1.45	2.5	1.75	2.25	1.55
OD, in.	2.2	1.575	2.6	1.83	2.45	1.70
Length, ft	10	10	10	10	10	10
Number	44	44	44	44	44	44
Flow Rate, lb/sec	15.1	4.72	15.1	4.72	30.1	9.48
Fluid Density, lb/sec	8.46	3.1	1.37	0.60	2.72	1.15
Dynamic Pressure, atm	0.416	0.403	1.05	0.976	3.21	2.89
Re_D	7.8×10^6	7.8×10^6	1.51×10^6	1.5×10^6	5.77×10^6	5.77×10^6
$(\Delta P/q)$ Friction	0.462	0.516	0.511	0.705	0.435	0.536
$(\Delta P/q)$ Turns	1.5	1.5	1.5	1.5	1.5	1.5
ΔP Total, atm	0.80	0.811	2.11	2.15	6.21	5.89
Inlet Pressure, atm	1002.2	1000.3	990.1	998.0	981.7	996.0
Inlet Temperature, deg R	898	898	4500	4500	2400	2400
Inlet Station	13	13	20	20	22	22
Volume, ft^3	2.02	1.08	1.62	0.696	2.26	1.17
Material Density, lb/ft^3	115.4	115.4	1204	1204	540	540
Material Weight, lb	233	125	1950	840	1359	702
Insulation OD, in.	2.5	1.875	3.1	2.33	-	-
Insulation Vol., ft^3	3.36	2.3	5.55	5.01	-	-
Insulation Density, lb/ft^3	124.8	124.8	124.8	124.8	-	-
Insulation Weight, lb	420	288	692	625	-	-
Total Weight, lb	653	413	2642	1465	1359	702

Total weight saving for Configurations D or E = 2075 lb

[redacted]

TABLE V

COMPARISON OF TOTAL WEIGHT EXCLUSIVE OF PRESSURE VESSEL AND TOTAL QUANTITY OF NEUTRON ABSORBING MATERIALS

Engine Configuration	Weight, lb				
	A	B	C	D	E
Moderator & Liner Tubes(1)					
Tungsten-184	1,171	50	50	50	50
Beryllium	2,611	2,760	2,760	2,760	2,760
Beryllium Oxide	9,530	9,530	10,980	9,530	10,980
Graphite	17,100	17,100	32,800	17,100	32,800
Pyrolytic Graphite	1,015	2,050	2,050	2,050	2,050
Heavy Water	18,750	18,750	0	18,750	0
Niobium Carbide	0	222	222	270	300
Piping	10,561	10,561	10,561	8,486	8,486
Heat Exchangers	13,462	13,462	13,162	8,200	7,900
Total	74,200	74,485	72,585	67,196	65,296
Neutron Absorbing Material					
Niobium Carbide					
Weight, lbs	0	222	222	270	300
Absorbing Area(2), cm^2	0	390	390	475	529
Tungsten-184					
Weight, lbs	1,171	50	50	50	50
Absorbing Area(2), cm^2	2,060	88	88	88	88
Total Absorbing Area, cm^2	2,060	478	478	563	617

(1) Includes all interior piping for moderator coolant and propellant

(2) Based on neutron absorbing area of 3.67×10^{-3} cm^2/gm for NbC and 3.86×10^{-3} cm^2/gm for W-184

[redacted]

TABLE VI

CONDITIONS IN CAVITY OF REFERENCE ENGINE DESIGN

Information Obtained from Ref. 4

Cavity diameter, D = 6.0 ft

Cavity length, L = 6.0 ft

Cavity volume, X = 169.5 ft^3

Cavity propellant flow, W_C = 236 lb/sec

Total propellant flow, W_T = 575 lb/sec

Critical mass, w_F = 18.1 lb

Cavity pressure, P = 1000 atm

Temperature at outside edge of fuel-containment region, T_6 = 102,000 R

Density at outside edge of fuel-containment region, ρ_6 = 0.0215 lb/ft^3

Viscosity at outside edge of fuel-containment region, $\mu_6 = 6.85 \times 10^{-5}$ lb/sec - ft

Time constant parameter evaluated using ρ and μ at Station 6, $(\rho/\mu)_6 r_1^2$ =2820 sec

Centerline temperature, T_8 = 136,000 R

Density of propellant at centerline conditions, ρ_8 = 0.0158 lb/ft^3

Viscosity of propellant at centerline conditions, $\mu_8 = 11.9 \times 10^{-5}$ lb/sec - ft

Time constant parameter, evaluated using centerline conditions, $(\rho/\mu)_8 r_1^2$ = 1195 sec

Axial-flow Reynolds number in full-scale engine (see Ref. 4), Re_z = 480,000

Cavity volume flow based on ρ_6, $Y_6 = W_C/\rho_6$ = 10,960 ft^3/sec

Minimum time constant based on ρ_6, $t_{F_{6_{MIN}}} = X/Y_6$ = 0.01546 sec

[redacted]

TABLE VII

RELATION BETWEEN VARIOUS MEASURES OF FUEL LOSS RATE

Information Obtained from Ref. 4 and Table VI

Criteria Governing Fuel Loss Rate	Fuel Time Constant, t_F, sec	Ratio of Fuel Time Constant to Minimum Fuel Time Constant, $t_F / t_{F_{6_{MIN}}}$	Dimensionless Time Constant Based on ρ_6 and μ_6, $\tau_{F_{1-6}} = t_F/(\rho/\mu)_6 r_1^2$	Dimensionless Time Constant Based on ρ_8 and μ_8, $\tau_{F_{1-8}} = t_F/(\rho/\mu)_8 r_1^2$	Fuel Flow, $W_F = w_F/t_F$ lb/sec	Ratio of Total Propellant Flow to Fuel Flow, W_T/W_F	$\frac{\text{(Fuel Cost)}}{\text{(Payload Weight)}}$, $\frac{\$}{\text{lb}}$	$\frac{\text{(Mission Cost)}}{\text{(Payload Weight)}}$, $\frac{\$}{\text{lb}}$
	①	② = ①/0.01546	③ = ①/2820	④ = ①/1195	⑤ = 18.1/①	⑥ = 575/⑤	⑦ = 21,500/⑥	⑧ = ⑦ + 225
Fully Mixed Flow Based on ρ_6	0.01546	1.0*	0.0000055	0.0000129	1171	0.49	43,877	44,102
Fuel Loss Rate to Provide Same Cost per lb of Payload as with Solid-Core Nuclear Rocket (see text)	0.308	19.92	0.000109	0.000258	58.8	9.76	2201	2426*
Fuel Loss Rate to Provide Cost per lb of Payload Equal to One-Third of that for Solid-Core Nuclear Rocket	1.160	75.0	.000411	0.000971	15.6	36.9	583	808*
Dimensionless Time Constant, $\tau_{F_{1-8}} = 0.01$	11.95	773	0.00424	0.01*	1.51	381	56.4	281
Ratio of Propellant Flow to Fuel Flow, $W_T / W_F = 1000$	31.5	2038	0.01117	0.0264	0.575	1000*	21.5	246

*Input value

PHOTOGRAPHS OF MULTIPLE-FIXED-PORT AND DIRECTED-WALL-JET VORTEX TUBES

a.) MULTIPLE-FIXED-PORT VORTEX TUBE, A_j = 13.1 SQ IN.

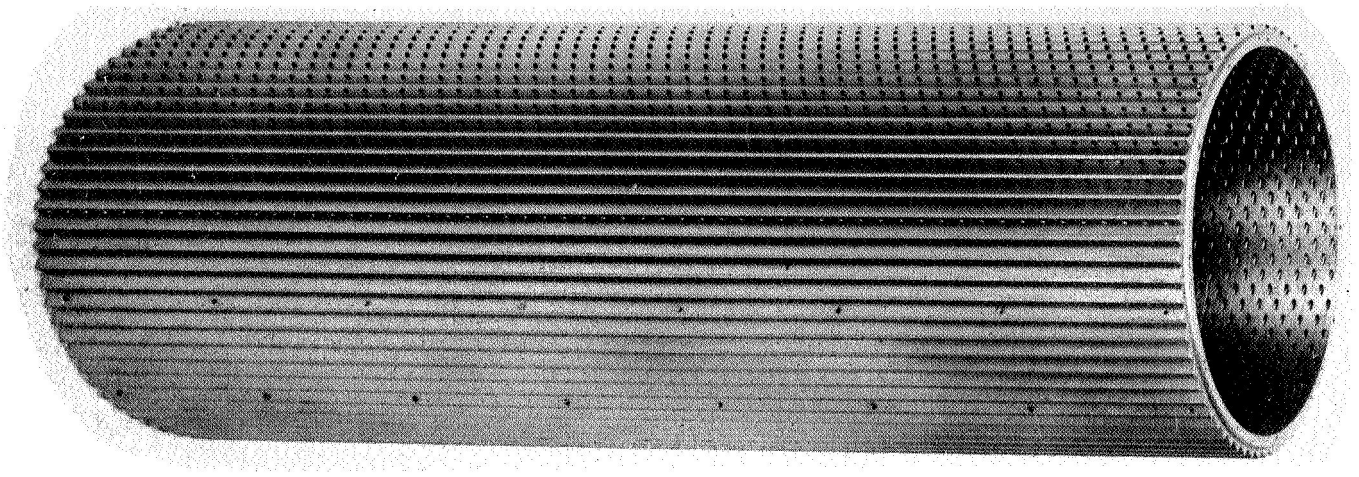

LENGTH, L = 30 IN. DIAMETER, D = 10 IN.

b.) DIRECTED-WALL-JET VORTEX TUBE, ALL JETS AT β_j = 45 DEG

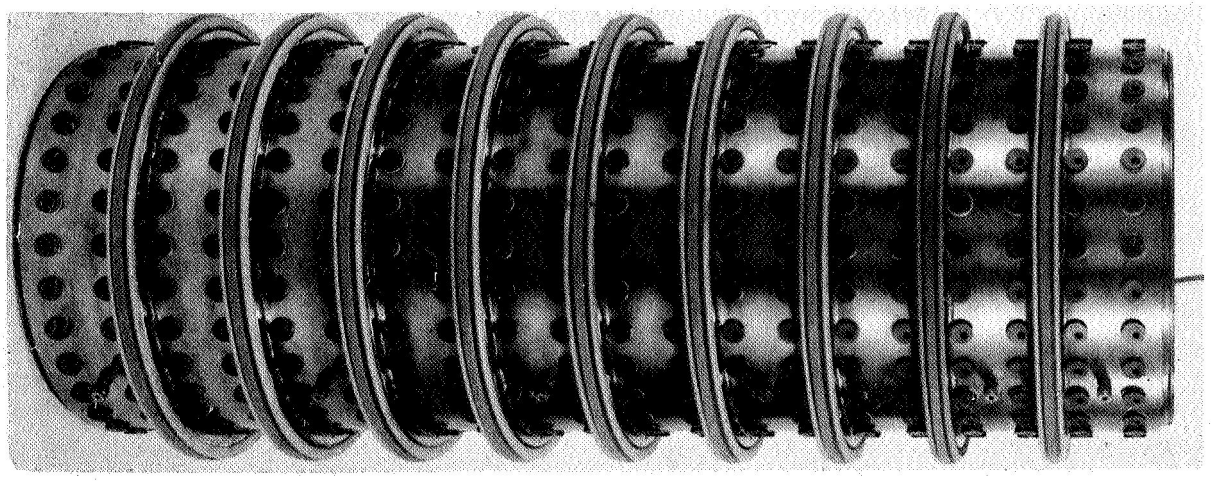

LENGTH, L = 30 IN. DIAMETER, D = 10 IN.

VARIATION OF DIMENSIONLESS TIME CONSTANT WITH HEAVY-GAS DENSITY RATIO FOR THE MULTIPLE-FIXED-PORT VORTEX TUBE HAVING A_j = 13.1 IN.^{2} AND L/D = 3.0

HEAVY-GAS INJECTION AT CENTER OF NONAXIAL-FLOW END WALL

VELOCITY RATIO, $\bar{V}_{z,w} / V_{\phi,j}$ = 0.38

ALL DATA FROM TESTS IN HIGH-REYNOLDS-NUMBER TEST FACILITY

SYMBOL	$Re_{z,w}$	$Re_{\phi,j}$	$\tau_{F_1\ MIN}$
D	46,000	121,000	0.00029
◇	73,600	194,000	0.00018
□	92,600	244,000	0.00015
△	133,000	350,000	0.00010

OPEN SYMBOLS - UPPER TRAVERSE

SOLID SYMBOLS - LOWER TRAVERSE

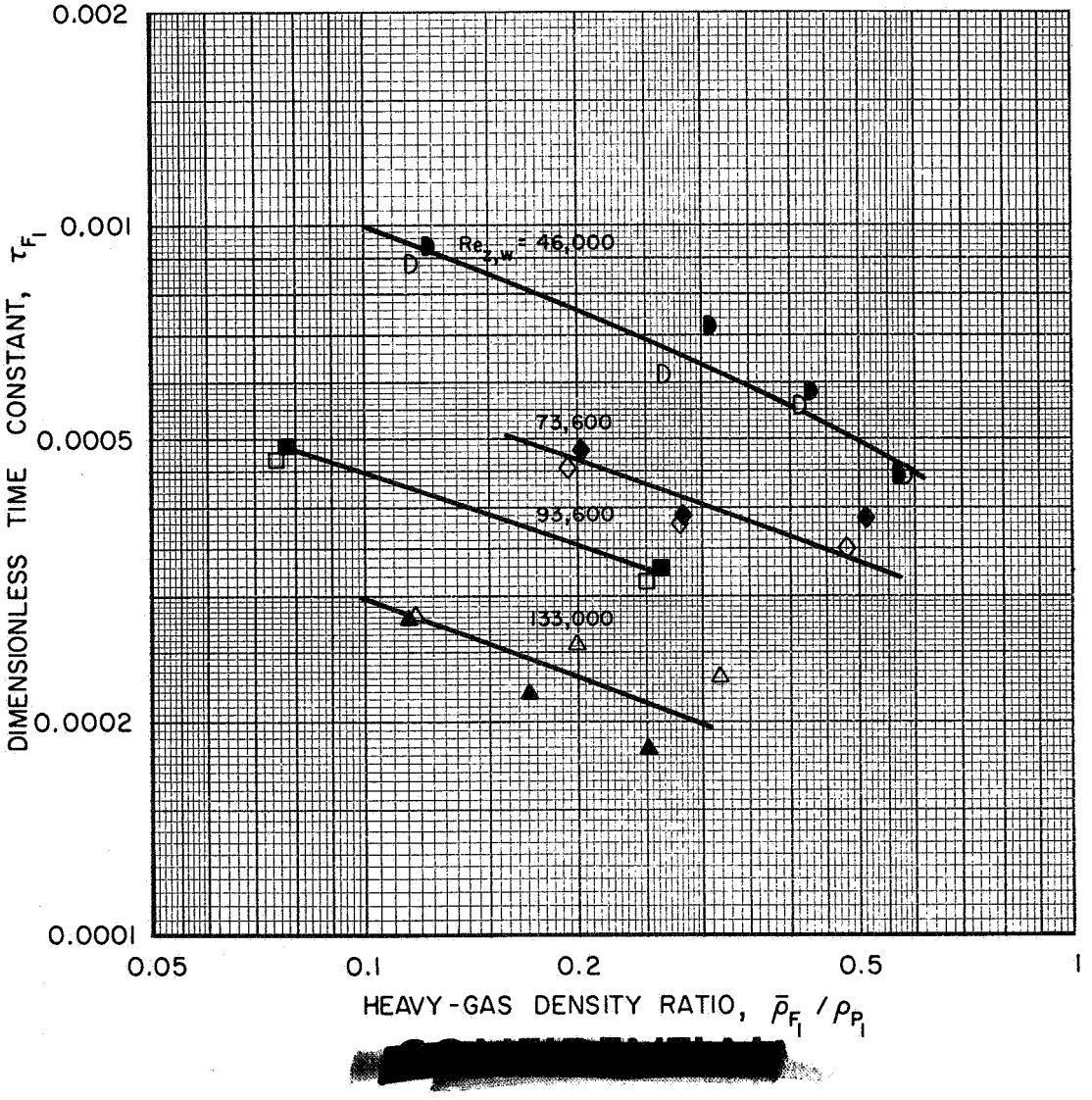

[redacted]

[redacted]

FIG. 3

VARIATION OF DIMENSIONLESS TIME CONSTANT WITH HEAVY-GAS DENSITY RATIO FOR THE MULTIPLE-FIXED-PORT VORTEX TUBE HAVING $A_j = 20.5$ IN.^{2} AND L/D = 3.0

HEAVY-GAS INJECTION AT CENTER OF NONAXIAL-FLOW END WALL

VELOCITY RATIO, $\bar{V}_{z,w} / V_{\phi,j} = 0.60$

ALL DATA FROM TESTS IN HIGH-REYNOLDS-NUMBER TEST FACILITY

SYMBOL	$Re_{z,w}$	$Re_{\phi,j}$	$\tau_{F_1\ MIN}$
D	49,000	81,600	0.00027
◇	101,000	169,000	0.00013
□	158,000	263,000	0.000086
△	199,000	332,000	0.000069
○	287,000	478,000	0.000048

OPEN SYMBOLS - UPPER TRAVERSE
SOLID SYMBOLS - LOWER TRAVERSE

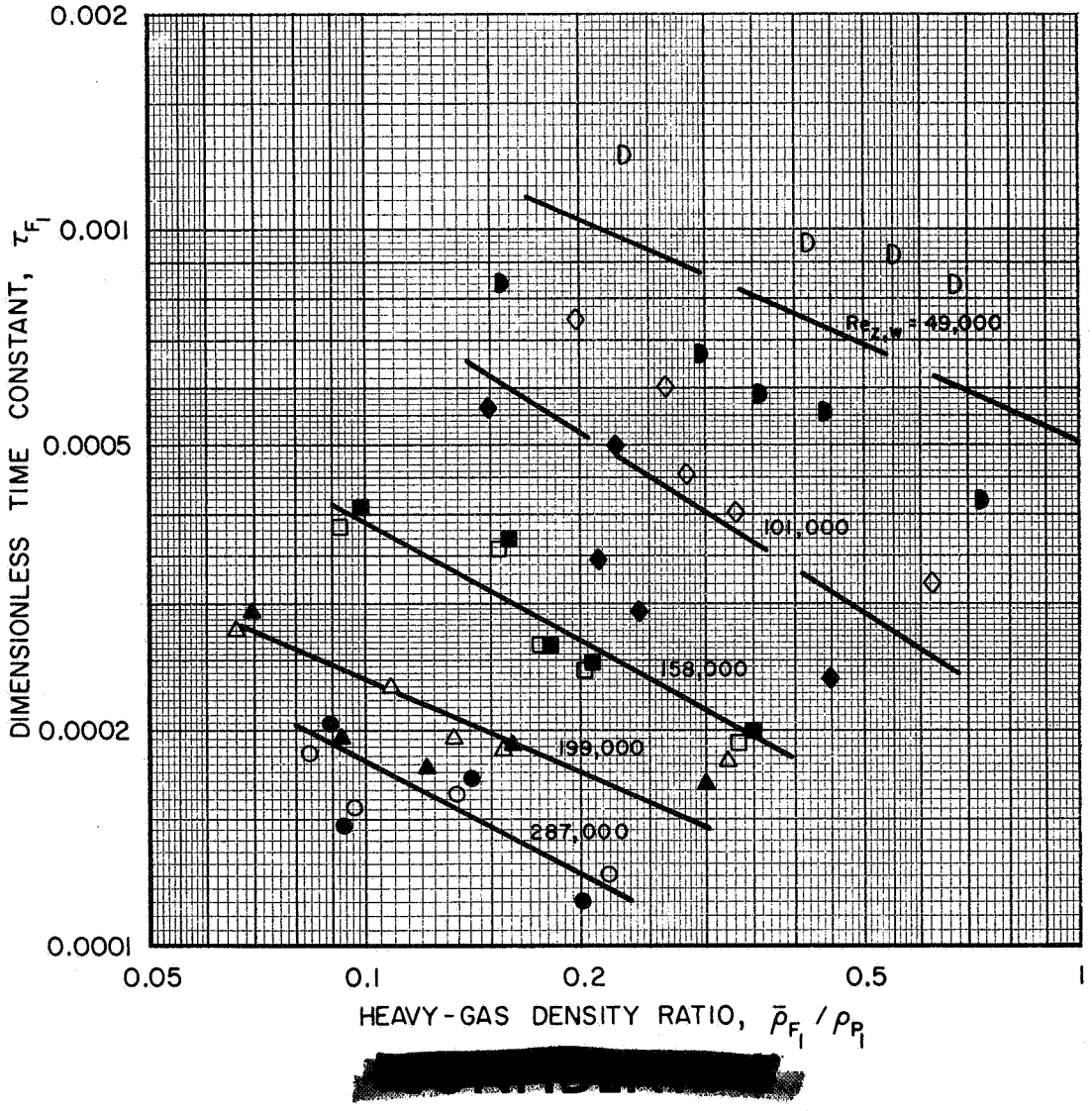

[redacted]

FIG. 4

VARIATION OF DIMENSIONLESS TIME CONSTANT WITH HEAVY-GAS DENSITY RATIO FOR THE MULTIPLE-FIXED-PORT VORTEX TUBE HAVING A_j = 40.2 IN.^{2} AND L/D = 3.0

HEAVY-GAS INJECTION AT CENTER OF NONAXIAL-FLOW END WALL

VELOCITY RATIO, $V_{z,w} / V_{\phi,j}$ = 1.16

ALL DATA FROM TESTS IN HIGH-REYNOLDS-NUMBER TEST FACILITY

SYMBOL	$Re_{z,w}$	$Re_{\phi,j}$	$\tau_{F_1\,MIN}$
D	48,600	41,900	0.00028
◇	100,000	86,100	0.00014
△	194,000	167,000	0.000071
□	285,000	247,000	0.000048
○	481,000	415,000	0.000029

OPEN SYMBOLS - UPPER TRAVERSE

SOLID SYMBOLS - LOWER TRAVERSE

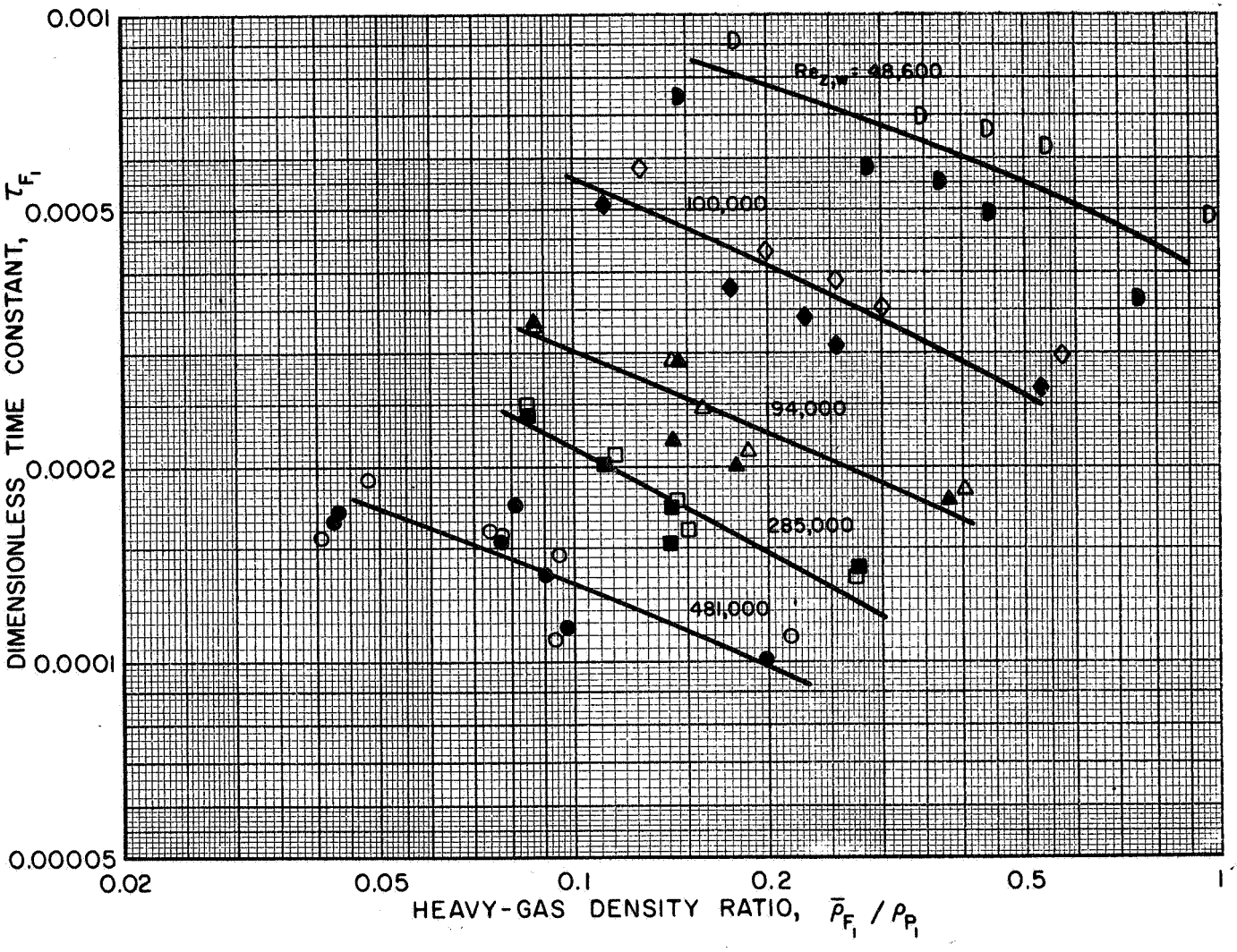

VARIATION OF DIMENSIONLESS TIME CONSTANT WITH HEAVY-GAS DENSITY RATIO FOR THE MULTIPLE-FIXED-PORT VORTEX TUBE HAVING A_j = 13.3 IN.^{2} AND L/D = 1.0

HEAVY-GAS INJECTION AT CENTER OF NONAXIAL-FLOW END WALL

VELOCITY RATIO, $V_{z,w} / V_{\phi,j}$ = 0.387

ALL DATA FROM TESTS IN HIGH-REYNOLDS-NUMBER TEST FACILITY

SYMBOL	$Re_{z,w}$	$Re_{\phi,j}$	$\tau_{F_{I\,MIN}}$
D	48,600	125,500	0.000093
◇	100,000	258,000	0.000045
□	157,000	406,000	0.000029
△	197,000	510,000	0.000023
O	348,000	902,000	0.000013

OPEN SYMBOLS - UPPER TRAVERSE

SOLID SYMBOLS - LOWER TRAVERSE

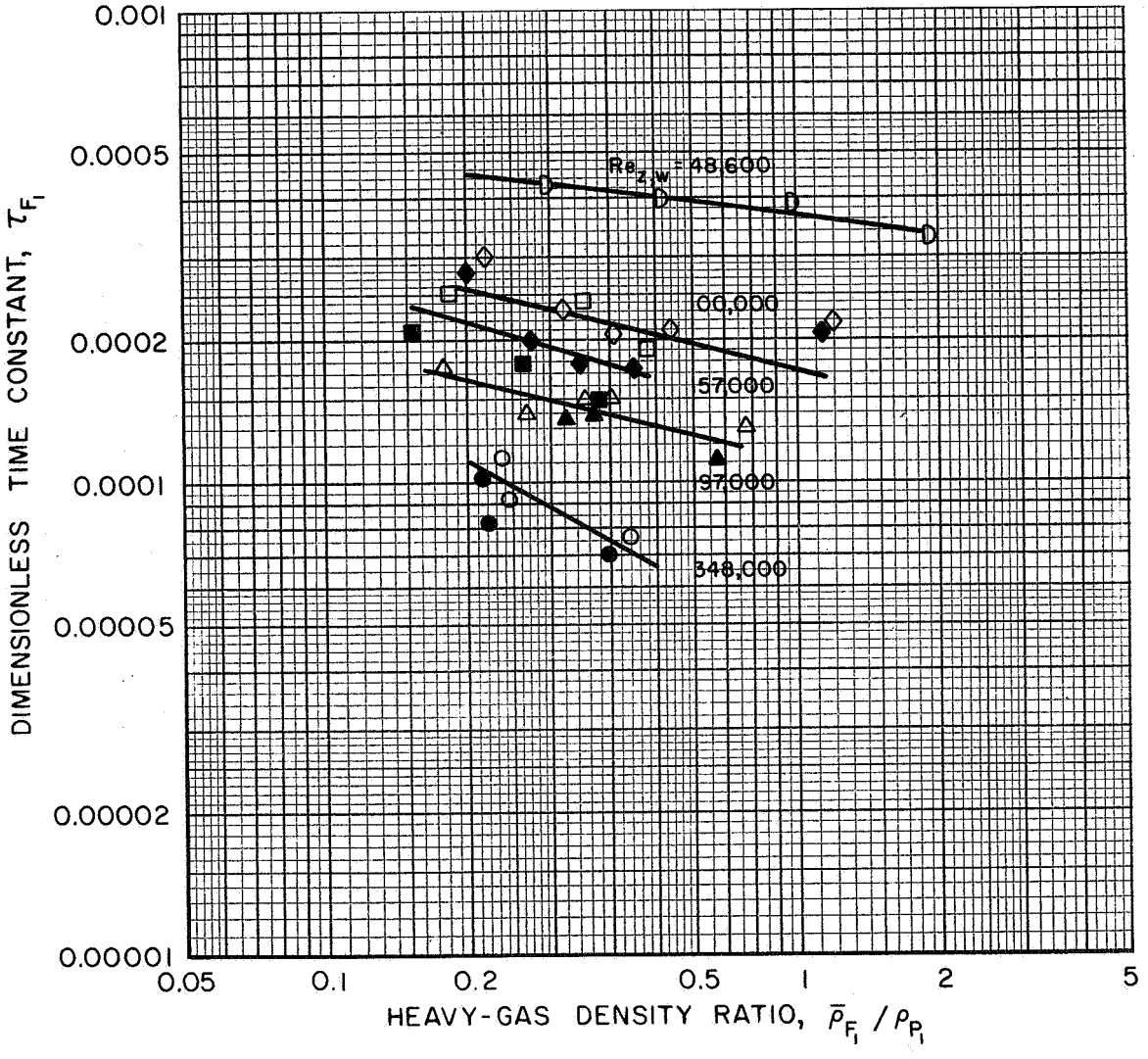

[redacted]

[redacted]

VARIATION OF DIMENSIONLESS TIME CONSTANT WITH AXIAL-FLOW REYNOLDS NUMBER FOR THE MULTIPLE-FIXED-PORT VORTEX TUBES

HEAVY-GAS INJECTION AT CENTER OF NONAXIAL-FLOW END WALL

HEAVY-GAS DENSITY RATIO, $\bar{\rho}_{F_1} / \rho_{P_1} = 0.2$

ALL DATA FROM TESTS IN HIGH-REYNOLDS-NUMBER TEST FACILITY

SYMBOL	A_j, IN.^{2}	$V_{z,w} / V_{\phi,j}$; $Re_{z,w} / Re_{\phi,j}$	L / D
◇	13.3	0.38	1.0
○	13.1	0.38	3.0
△	20.5	0.60	3.0
□	40.2	1.16	3.0

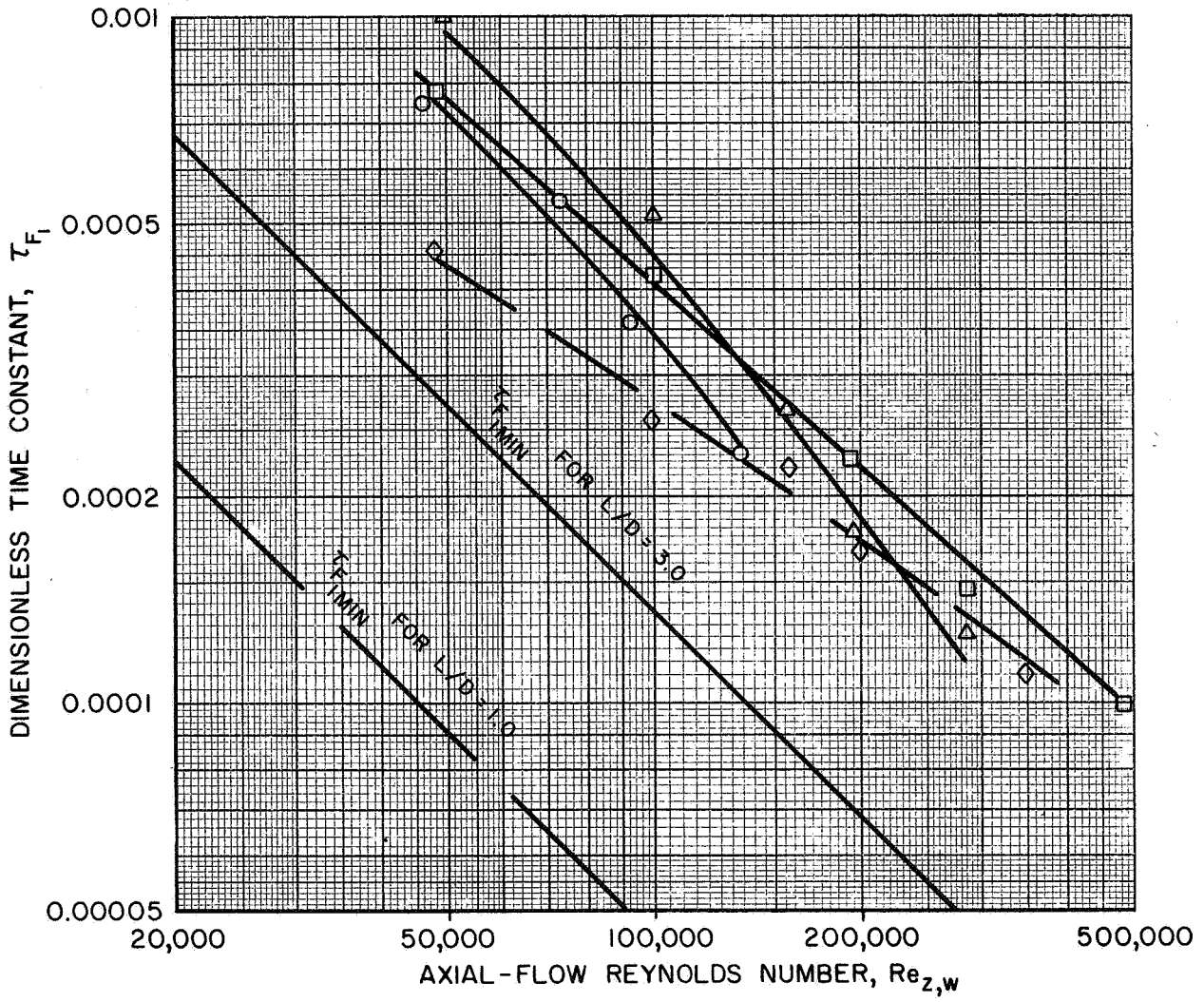

[redacted]

[redacted]

VARIATION OF CONTAINMENT PARAMETER WITH AXIAL-FLOW REYNOLDS NUMBER FOR THE MULTIPLE-FIXED-PORT VORTEX TUBES

HEAVY-GAS INJECTION AT CENTER OF NONAXIAL-FLOW END WALL

HEAVY-GAS DENSITY RATIO, $\bar{\rho}_{F_1} / \rho_{P_1} = 0.2$

ALL DATA FROM TESTS IN HIGH-REYNOLDS-NUMBER TEST FACILITY

SYMBOL	A_j - IN.^{2}	$\bar{V}_{z,w} / V_{\phi,j}$; $Re_{z,w} / Re_{\phi,j}$	L / D
○	13.3	0.38	1.0
△	13.1	0.38	3.0
◇	20.5	0.6	3.0
□	40.2	1.16	3.0

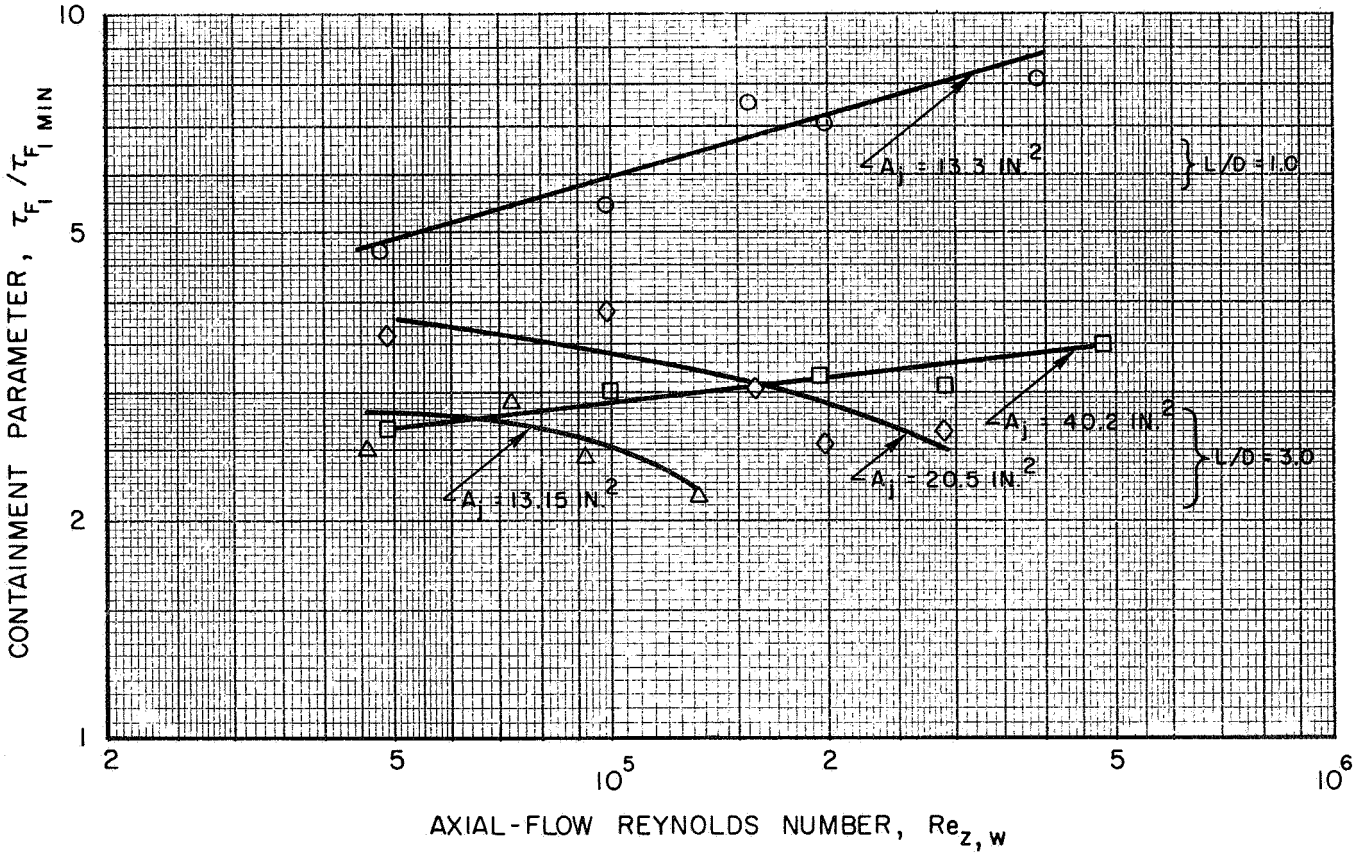

[redacted]

CORRELATION OF THE CONTAINMENT PARAMETER WITH THE VELOCITY RATIO $\bar{V}_{z,w} / V_j$ FOR SEVERAL LIGHT-GAS INJECTION CONFIGURATIONS

AXIAL-FLOW REYNOLDS NUMBER, $Re_{z,w} = 5.0 \times 10^4$

HEAVY-GAS DENSITY RATIO, $\bar{\rho}_{F_1} / \rho_{P_1} \cong 0.15$

HEAVY-GAS INJECTION AT CENTER OF NONAXIAL-FLOW END WALL, EXCEPT AS NOTED

DATA FROM BOTH HRN AND DWJ TEST FACILITIES

SYMBOL	LIGHT-GAS INJECTION CONFIGURATION	L/D	TEST FACILITY	$Re_{\phi,j}$
○	MULTIPLE-FIXED-PORT	3.0	HRN	$Re_{\phi,j} = Re_{z,w} (V_j / \bar{V}_{z,w})$
◐	TAPED-MULTIPLE-FIXED-PORT	3.0	HRN	
●	TAPED-MULTIPLE-FIXED-PORT	3.0	DWJ	
⊗	MULTIPLE-FIXED-PORT	1.0	HRN	
□	DWJ - ALL 0 DEG	3.0	DWJ	
⊠	DWJ - 0 TO 45 DEG	3.0	DWJ AND HRN	158,000
■	DWJ - 0 TO 63.5 DEG	3.0	DWJ	158,000

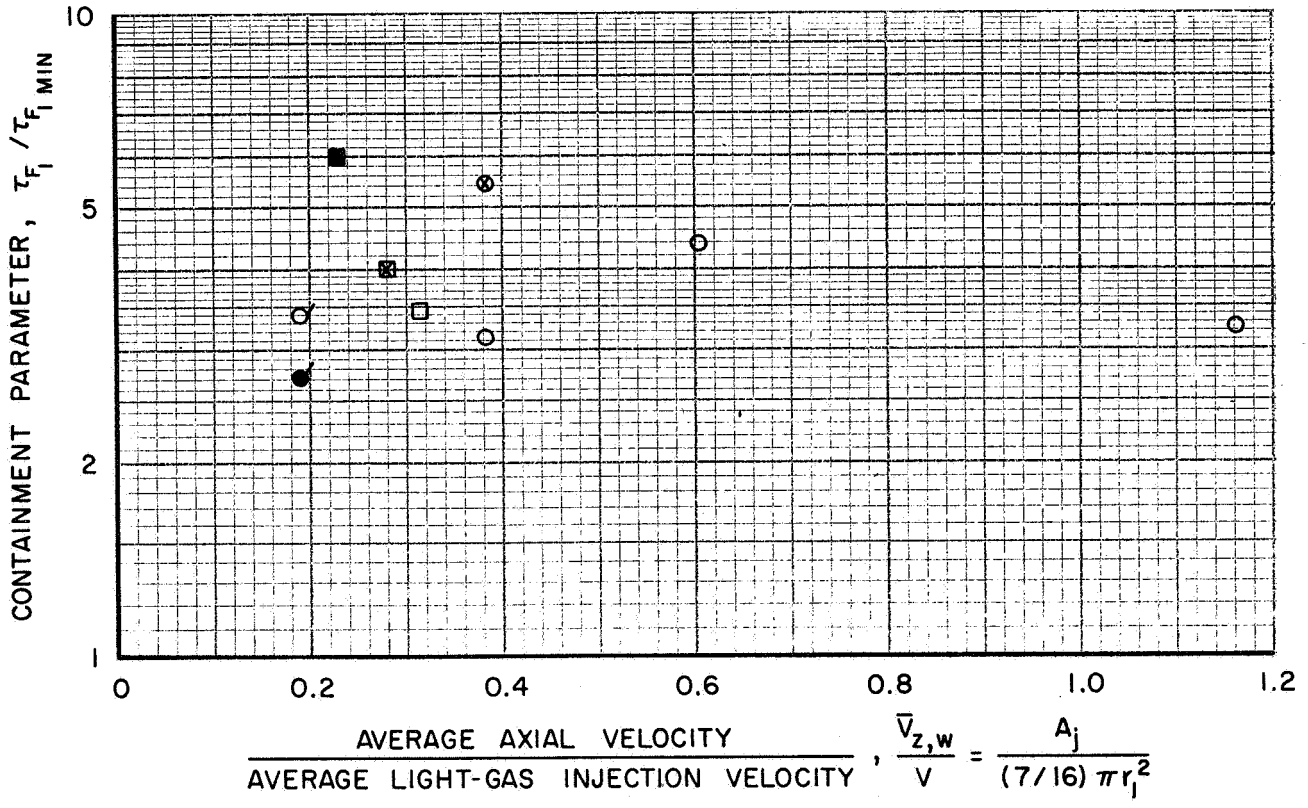

[redacted]

EFFECT OF AXIAL-FLOW EXHAUST ANNULUS GEOMETRY ON CONTAINMENT CHARACTERISTICS FOR A MULTIPLE-FIXED-PORT VORTEX-TUBE CONFIGURTION

LENGTH-TO-DIAMETER RATIO, L/D = 3.0
AXIAL-FLOW REYNOLDS NUMBER, $Re_{z,w} = 7.4 \times 10^4$
LIGHT-GAS INJECTION AREA, A_j = 13.1 IN.^{2}
LIGHT-GAS TANGENTIAL INJECTION REYNOLDS NUMBER, $Re_{\phi,j} = 19.2 \times 10^4$
HEAVY-GAS INJECTION CONFIGURATION AT CENTER OF NONAXIAL-FLOW END WALL
ALL DATA FROM TESTS IN HIGH-REYNOLDS-NUMBER TEST FACILITY

SYMBOL	RADIAL EXTENT OF ANNULUS, IN.	STRUTS PRESENT
○	4.5 → 5.0	NO
△	4.0 → 5.0	NO
□	4.0 → 5.0	YES

OPEN SYMBOLS - UPPER TRAVERSE
SOLID SYMBOLS - LOWER TRAVERSE

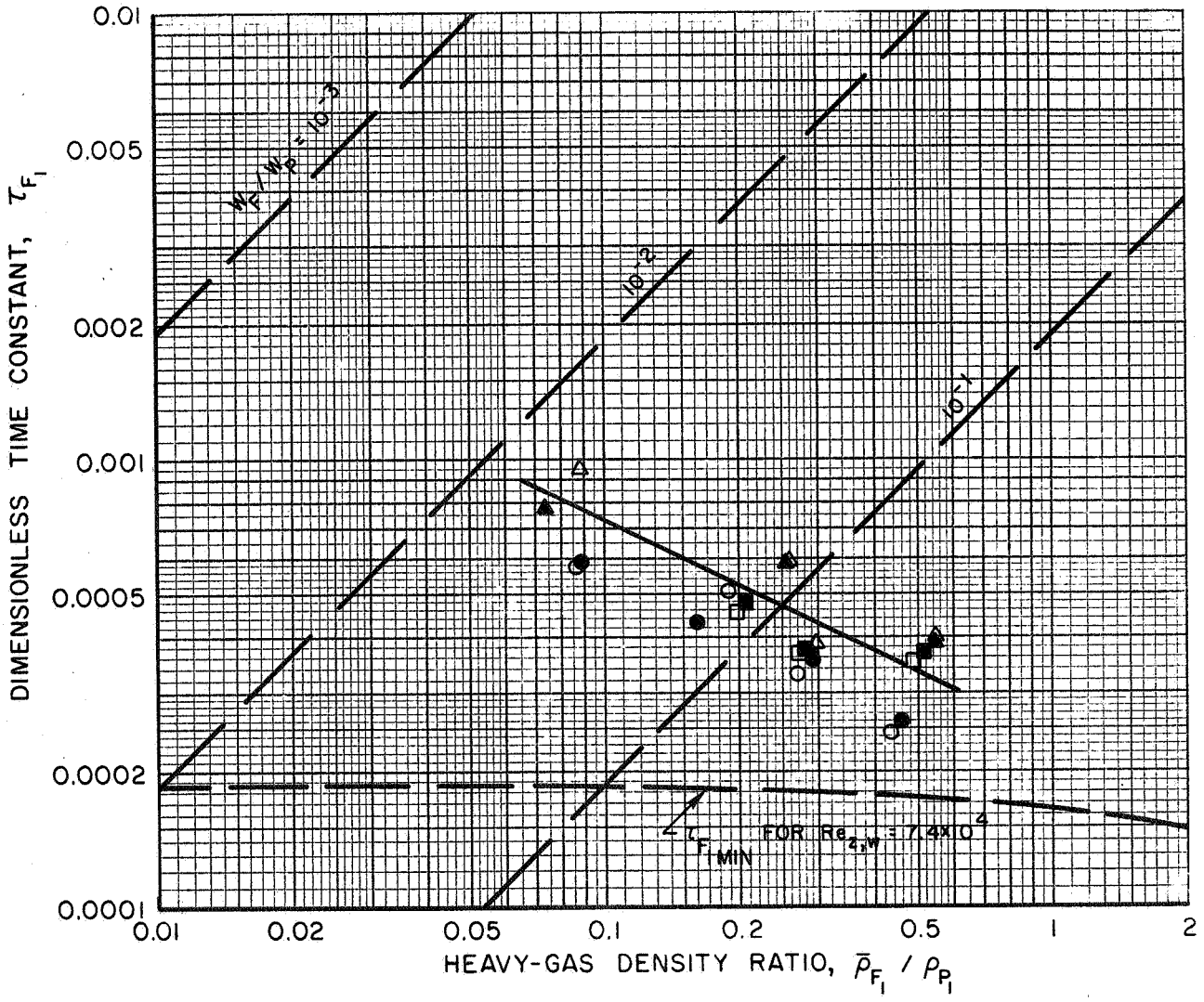

[redacted]

[redacted]

EFFECT OF HEAVY-GAS INJECTION WITH SWIRL ON CONTAINMENT PARAMETER $\tau_{F_I} / \tau_{F_{I\,MIN}}$

LENGTH-TO-DIAMETER RATIO, L/D = 3.0

LIGHT-GAS INJECTION CONFIGURATION, DWJ - 0 TO 45 DEG

AXIAL-FLOW REYNOLDS NUMBER, $Re_{z,w} \approx 42{,}000$

LIGHT-GAS TANGENTIAL INJECTION REYNOLDS NUMBER, $Re_{\phi,j} \approx 135{,}000$

DIMENSIONLESS TIME CONSTANT FOR FULLY MIXED FLOW, $\tau_{F_{I\,MIN}} = 0.00032$

SYMBOL	HEAVY-GAS INJECTION CONFIGURATION	$A_{F,j}$ - IN.^{2}
◇	NO SWIRL; 0.9-IN.-DIA DUCT AT NONAXIAL-FLOW END WALL	0.634
□	SWIRL; 4 - 0.060 IN. x 0.3 IN. JETS AT 0.43-IN. RADIUS 8 - 0.1 IN. 0.5 IN. JETS AT 1.12-IN. RADIUS	0.475

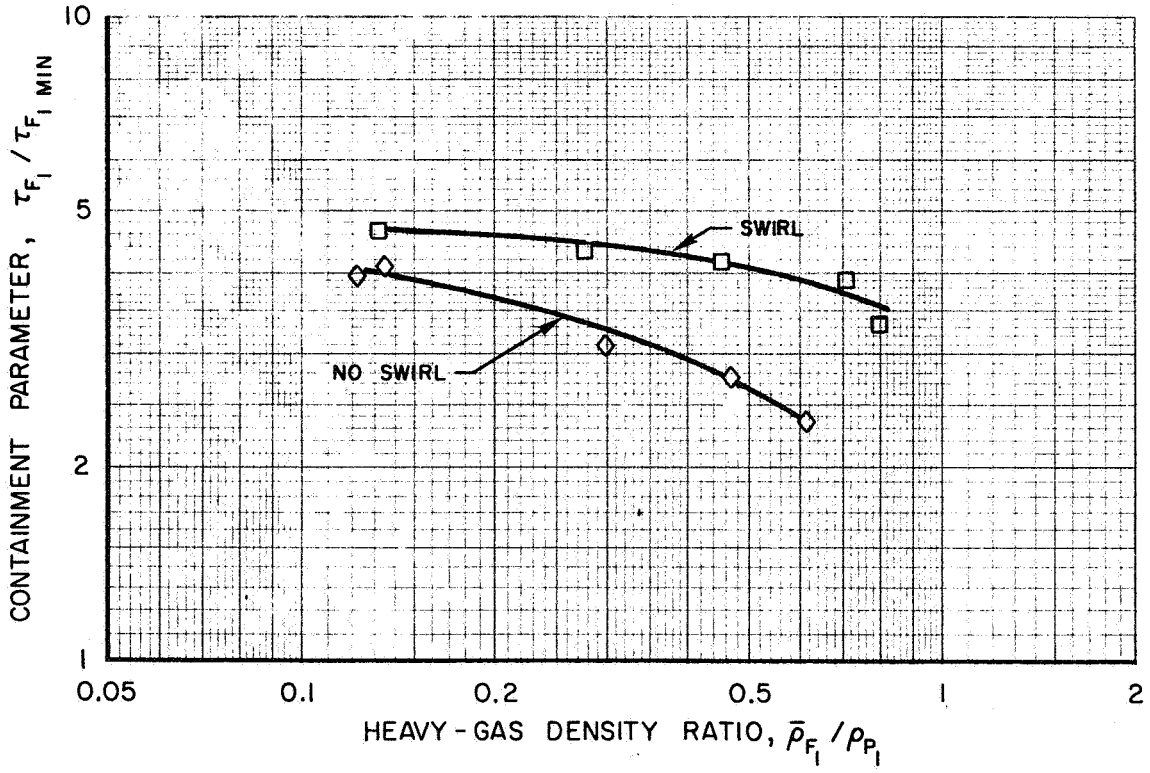

[redacted]

[redacted]

COMPARISON OF TANGENTIAL VELOCITY PROFILES IN 2144-PORT-INJECTION AND ROTATING-STABILITY VORTEX TUBES AT OUTFLOW RADIAL REYNOLDS NUMBER OF $Re_r = -30$

FLUID INJECTION THROUGH STATIONARY CENTERLINE POROUS TUBE

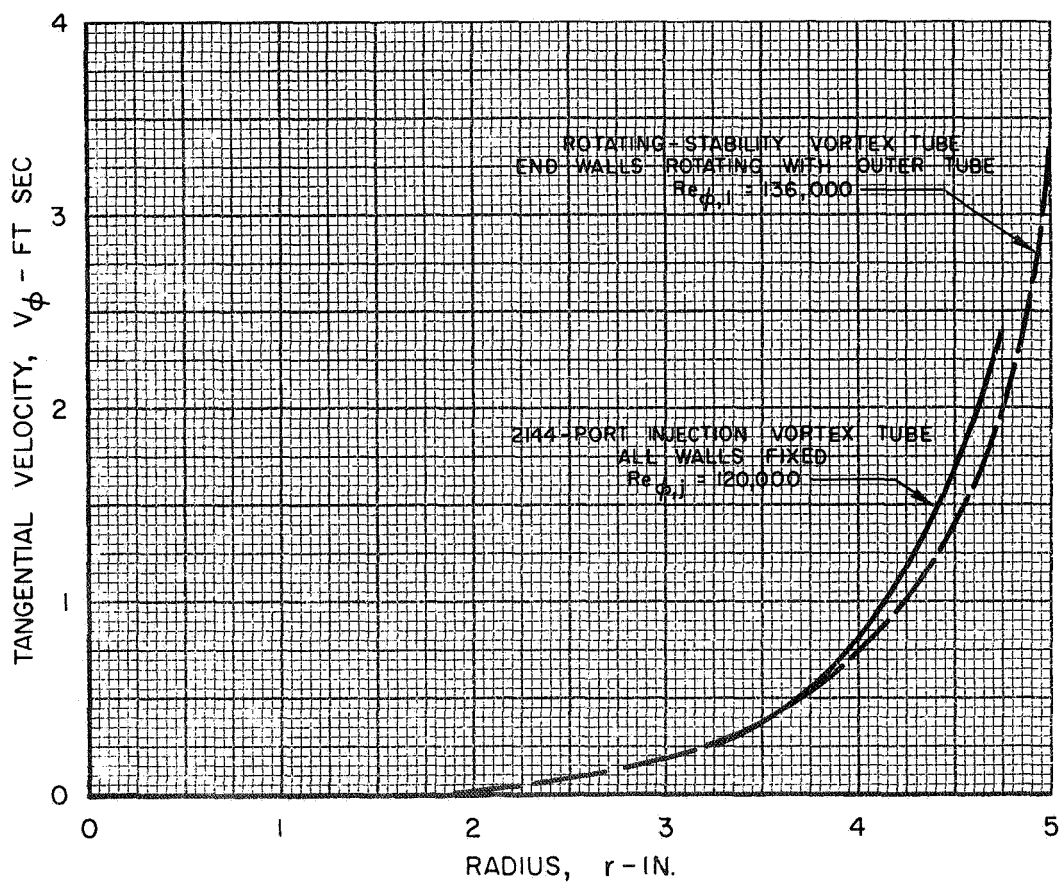

[redacted]

E-910093-31

SKETCH OF TYPICAL LAMINAR STREAMLINE PATTERN IN ROTATING-STABILITY APPARATUS - FLUID INJECTION THROUGH STATIONARY INNER POROUS TUBE - END WALLS ROTATING WITH OUTER TUBE

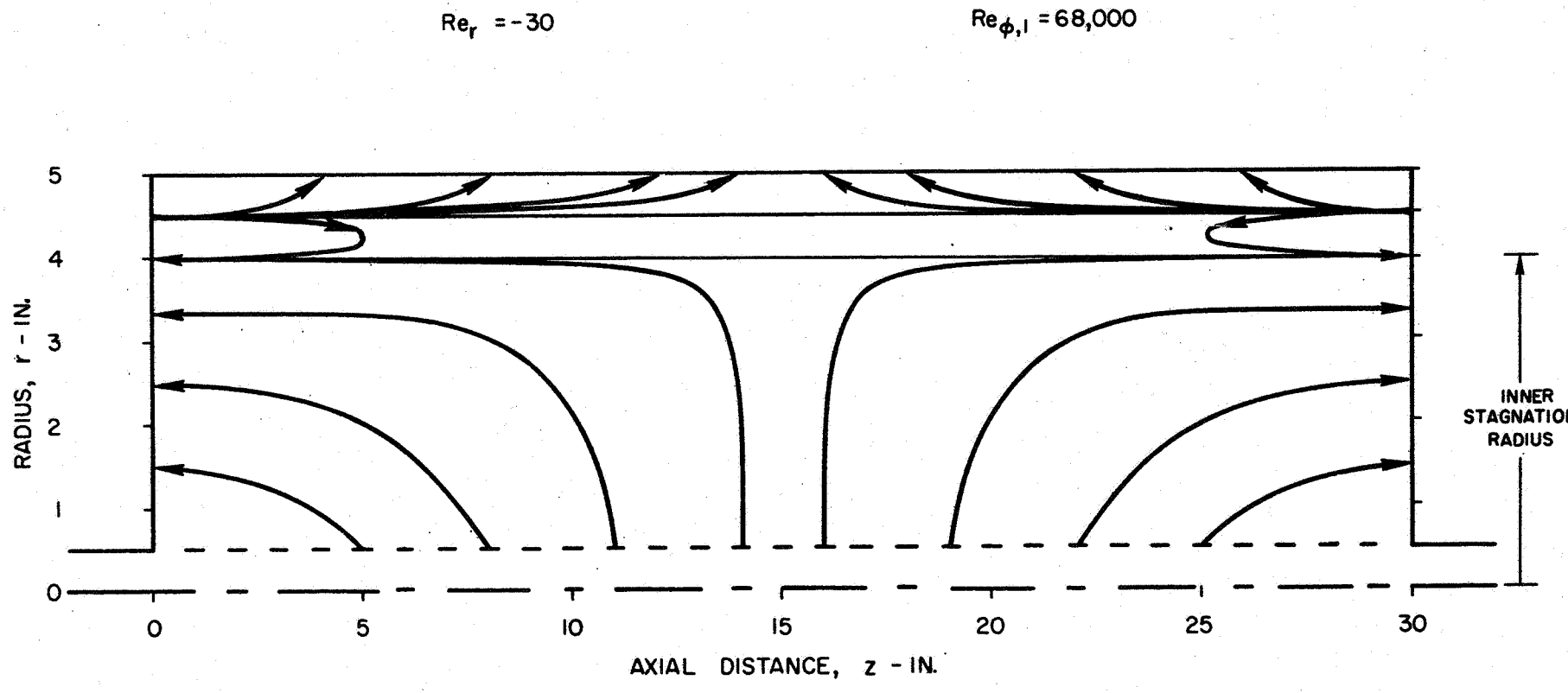

FIG. 12

VARIATION OF NIOBIUM CARBIDE COATING WEIGHT AND TOTAL PRESSURE DROP IN GRAPHITE MODERATOR WITH COOLANT HOLE DIAMETER

ENGINE CONFIGURATION D

NIOBIUM THICKNESS ON SURFACE OF GRAPHITE TO PROTECT GRAPHITE FROM ATTACK = 0.002 IN.

SPIRAL COOLING HOLES

GRAPHITE THICKNESS = 8.7 IN.

AVERAGE VOLUMETRIC HEAT DEPOSITION = 1.092×10^4 BTU/SEC-FT^3

COOLANT TO WALL TEMPERATURE DIFFERENCE = 200 R

MAXIMUM TO WALL TEMPERATURE DIFFERENCE = 100 R

COOLANT VOLUME FRACTION = 0.02

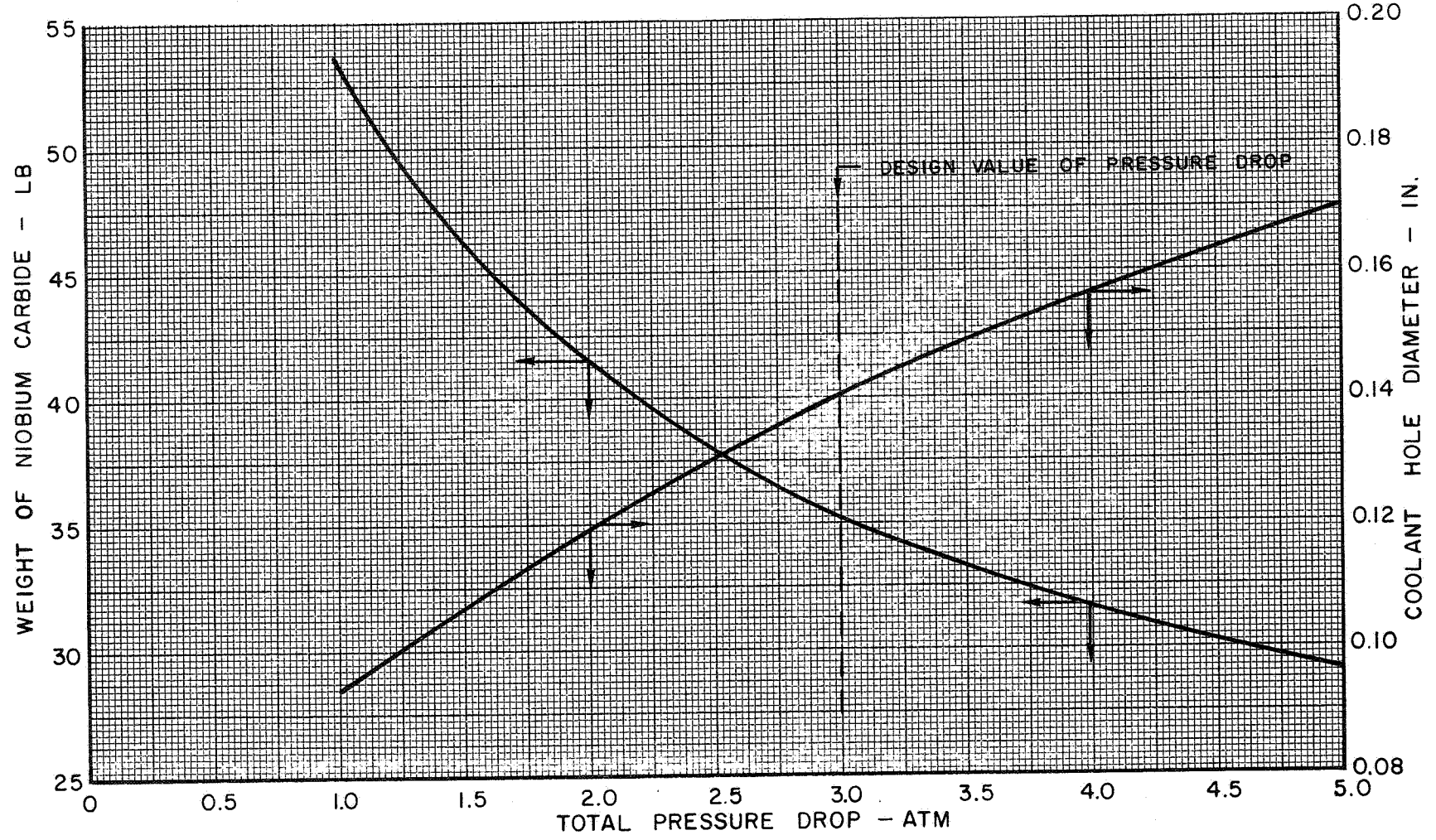

E-910093-31

FIG 13